Supporting Information

Chen et al. 10.1073/pnas.0900343106

SI Methods

Construction of Targeting Vector. We screened the CITB mouse BAC library (Invitrogen) with *Hras* gene-specific primers to obtain a BAC containing the entire mouse *Hras* gene. We then used recombineering (1) to introduce a DNA fragment containing the entire *Hras* gene and 2.3 kb upstream of *Hras* exon 0 (5′ arm) or a fragment consisting of the entire *Hras* gene and 2.5 kb downstream of *Hras* exon 4 (3′ arm) into pBSIISK+ or pBSIIKS+ (Stratagene), respectively. To complete the 5′ arm of the targeting construct, a *loxP* site was introduced upstream of exon 1, and a SV40 poly(A)/translation stop signal was placed 3′ of *Hras* exon 4. To complete the 3′ targeting arm, we used site-directed mutagenesis to change the nucleotide sequence at codon 12 to valine, and replaced exon 0 with a *Frt*-flanked *Neo* cassette with a 3′ *loxP* site added upstream of exon 1. The final targeting construct was generated by ligating the 5′ and 3′ arms, and was ≈11.8 kb in size (see Fig. 1).

Development of *FR-Hras^{G12V}* Mice. The targeting construct was transfected into 2 different 129SvEv (129S6) ES cell lines. Neo-resistant colonies were isolated and screened by PCR using a primer pair spanning the *Neo* gene and a site located just outside the 3′ targeting arm (primer sequences available on request). Appropriate integration was confirmed by Southern blotting. We then designed PCR primers to sequence all exons of both tandem *Hras* gene cassettes, including the exon 1 with the G12V mutation, the 5′, and 3′ *loxP* and *Frt* sites, respectively. One clone (D14) was found to have appropriate targeting of *Hras* and another (D61) was also properly targeted, but had a second integration site. These were then injected into D2B6F1 X B6 (Jackson Labs) blastocysts to produce chimeric mice. The chimeras were then bred to Swiss-Black (Taconic) females. The birth of agouti colored mice indicated germline transmission of ES cell-derived gametes. The agouti pups were genotyped to determine those that carried the targeted allele, resulting in 6 and 18 mice from clones D14 and D61, respectively. The founders were crossed with WT Swiss-Black mice and resulting pups were screened for *Hras* targeting. Founders from both lines had targeted offspring. An attempt to breed out the second integration site in D61 lines was not successful, and this line was therefore not further pursued. We reconfirmed the appropriate targeting and sequence integrity of the targeted allele in F1 pups from line D14, as described above. To remove the *Neo* cassette, *FR-Hras^{G12V}-Neo* mice were crossed with *β-actin-Flp* mice. The resulting double transgenic offspring were crossed with WT littermates. Offspring containing the *FR-Hras^{G12V}* allele without the *Neo* cassette and that were negative for *β-actin-Flp* were mated with WT littermates and the line expanded. We used advance intercross breeding to minimize drift in the genetic background.

Clinical and Anatomical Pathology. All mouse experiments were approved by the Institutional Animal Care and Utilization Committees of the University of Cincinnati and Memorial Sloan-Kettering Cancer Center. Mice were killed by CO_2 asphyxiation. Whole blood was collected postmortem by cardiac puncture, and complete blood counts and white blood-cell differentials were performed on EDTA anticoagulated whole blood. Aliquots of serum were submitted to a commercial reference laboratory (ALX Laboratory at Animal Medical Center, New York, NY) for determination of biochemical parameters. Body and select organ weights were obtained. Complete postmortem evaluations were performed on all mice. All tissues were fixed in 4% paraformaldehyde or 10% neutral buffered formalin for 24 h and then transferred to 70% ethanol, with the exception of the skull, vertebral column, and rear leg, which were fixed in Decalcifier I (Surgipath Medical Industries, Inc.) for 72 h. All tissues were processed by routine methods and embedded in paraffin wax. Sections (5 μm) were stained with H&E, and evaluated with an Olympus BX45 light microscope (New York/New Jersey Scientific, Inc.).

IHC Staining of Mouse Tissues. Tissues were promptly excised after killing, and either placed in a 4% PFA solution overnight at 4 °C and embedded in paraffin or immediately frozen with dry ice for frozen sectioning. Next, 5-μm paraffin sections were immunostained with antibodies to *p*-AKT (AF887, R&D Systems), Ki67 (VP-K451, Vector Laboratories), pERK (4376) and phospho ribosomal S6 kinase (2211L) from Cell Signaling, p53 (SC-6243), γH2AX (07–164, Upstate), and Dcr2 (AAP-371, Assay Designs, Inc.) with the help of the Memorial Sloan Kettering Cancer Center Molecular Cytology Core Facility. Staining for SA-βgal was performed using Biovision's senescence detection kit according to manufacturer's instruction (Biovision).

Laser-Capture Microdissection. Mouse stomach was promptly excised after killing and immediately frozen with liquid N2. Frozen sections (8 μm) were used to microdissect forestomach and glandular stomach epithelial cells by laser capture using an Arcturus microdissection system. RNA was extracted using a Picopure RNA Isolation Kit (Molecular Devices). Ras isoform, progastricsin, and keratin 5 mRNA levels were analyzed by real-time RT-PCR, standardized to GAPDH. Primers are available upon request.

MicroCT Imaging. For imaging, animals were anesthetized by continuous inhalation of a mixture of 1.5% isoflurane in air at a flow rate of 1 to 2 L/min and placed supine on the scanner couch. Ungated whole-body CT images were acquired without contrast using a dedicated small-animal CT scanner (MicroCAT-IITM, ImTek). The X-ray tube voltage was fixed at 55 kVp and the current at 800 ìA. A 360°-acquisition was performed over ≈12 min in 1° steps; each projection image was ≈1 sec in duration. The resulting projection-image data were reconstructed in real-time using the manufacturer-provided Feldkamp conebeam algorithm in a 192 × 192 × 384 3-dimensional image matrix (reconstructed voxel dimensions: 0.228 × 0.228 × 0.228 mm). The reconstructed images were then imported into ASIPro (Siemens Preclinical Solutions) for display and analysis.

Isolation of MEFs. MEFs were isolated from E13.5-day embryos as described (2). The fetal heads were used for genotyping. Cells were grown to confluence and split once before freezing, and labeled as passage 1. To determine cumulative cell counts after serial passaging, MEFs (10^6) of the indicated genotypes from passage 3 onwards were plated on 10-cm dishes, grown in 10% FCS for 3 days, trypsinized, counted, and replated at 10^6 cells per well. This was repeated for each passage. The cumulative cell number was calculated based on the formula $T^n = T^{n-1} x P^n/10^6$, where T = cumulative cell number; n = passage number; P = cell number of current passage after 3 days in culture. For short-term growth curves, MEFs at passages 3 and 15 were plated at 5×10^4, grown in 2% FCS, and counted every other day for 7 days.

Assay for Activated Hras. The Ras activation assay was performed using an agarose-bound GST-fused RBD of Raf-1 as instructed by the manufacturer (Upstate). Briefly, MEFs grown in 10% FCS were washed with cold PBS and lysed. The activated Ras was pulled down with agarose-conjugated Raf-1 RBD, followed by SDS/PAGE gel electrophoresis and immunoblotting with a specific anti-Hras antibody (sc-520, Santa Cruz Biotechnology).

Western Blotting. Cells were washed 3 times with ice-cold PBS and lysed in RIPA buffer containing a mixture of protease and phosphatase inhibitors (Sigma). Cell lysates were cleared by centrifugation. Tissue samples were homogenized and lysed with the same buffers, and following centrifugation, soluble protein was quantified by the Bradford method. Samples were subjected to 4 to 12% SDS/PAGE gradient gel (Invitrogen) and transferred to PVDF membrane. Western blots were performed according to standard procedures. The following antibodies were used: *p*-AKT (9271), total AKT (9272), *p*-FRS2 (3864) and *p*-ERK (9101) from Cell Signaling ; Erk2 (C-14), Hras (sc-520), p16 (sc-1207), p21 (sc-6246) and p53 (sc-6243) from Santa Cruz; Sprouty2 (ab50317), Spred2 (ab50535),p19 (ab80) from Abcam; β-actin (A1978) from Sigma.

1. Copeland NG, Jenkins NA, Court DL (2001) Recombineering: A powerful new tool for mouse functional genomics. *Nat Rev Genet* 10:769–779.
2. Serrano M, Lin AW, McCurrach ME, Beach D, Lowe SW (1997) Oncogenic ras provokes premature cell senescence associated with accumulation of p53 and p16INK4a. *Cell* 88:593–602.

Determination of Mutation Frequency in Vivo. Mutation frequency was determined using a plasmid rescue procedure applied to genomic DNA derived from thyroid tissues of ≈7-week-old *TPO-Cre/FR-Hras*$^{G12V\pm}$*/pUR288-LacZ* mice. Plasmids were recovered from mouse thyroid genomic DNA by restriction digestion and magnetic bead separation. After ligation, plasmids were electroporated into *E. coli C* (Δ*LacZ, gal E-)*. Transformants were plated in titration plates (containing X-gal), and *LacZ*-mutant plates (containing P-gal). Only *Lac-Z* mutants can form colonies in the presence of P-galactose, as described (3). Mutant frequency was obtained as the ratio of colonies in selective plates versus titration plates. The type of mutation was further determined by PCR amplification and restriction digestion of *LacZ*-negative clones, to discriminate between point mutations or large-scale events, such as recombinations.

Transformation Assays. Early passage MEFs were transduced with MSCV-IRES-puromycin vectors expressing cMyc, T antigen, or Hras^{G12V}, as indicated, or with empty vector. Transduced cells (5×10^6) were plated on 10-cm plates and maintained for 14 days, with media changed every 2 days. Foci were scored after staining with crystal violet.

3. Boerrigter ME, Dolle ME, Martus HJ, Gossen JA, Vijg J (1995) Plasmid-based transgenic mouse model for studying in vivo mutations. *Nature* 377:657–659.

Fig. S1. Tissue-specific activation of MEK-ERK in liver of *CC/FR-Hras*^{G12V} mice. (*A*) Western blots of the indicated tissues from 12-month-old *CC/FR-Hras*^{G12V} and control mice for the indicated proteins. There was a marked increase pERK and pMEK in livers from *CC/FR-HRas*^{G12V} mice compared to controls. No difference in pMEK, pERK, or pAKT was observed in brain, colon, kidney (or lung, not shown). (*B*) The liver-specific activation of MEK and ERK was confirmed in 8-day-old *CC/FR-Hras*^{G12V} mice, whereas no changes were found in the heart. (*C*) Western blots of brain and liver lysates from *CC/FR-Hras*^{G12V} and control mice probed with anti-Sprouty-2 IgG, Spred2 IgG, or β-actin IgG. Expression of Sprouty-2 was markedly lower in liver than in brain. By contrast, Spred2 was less abundant in brain than in liver.

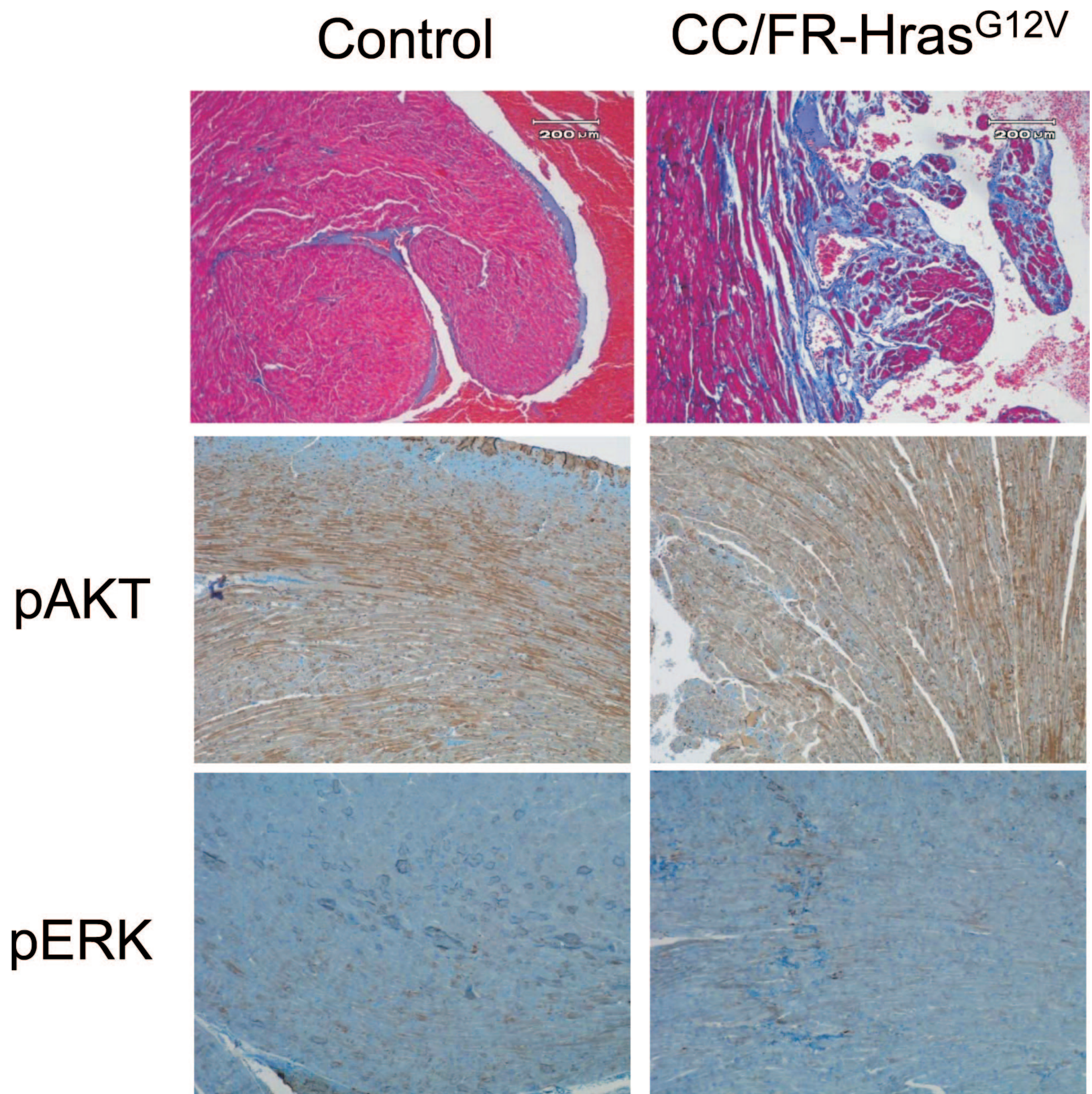

Fig. S2. *CC/FR-Hras*^{G12V} mice develop myocardial fibrosis. (*Top*) Trichrome staining (50×) of hearts from ≈52-week-old *CC/FR-Hras*^{G12V} and control mice. Myocardial fibrosis was found in 5 out of 6 *CC/FR-Hras*^{G12V} mice, but not in age-matched control mice (0 out of 6). Immunohistochemistry (IHC) of heart sections (50×) from 52-week-old *CC/FR-Hras*^{G12V} or control mice for pAKT (*Middle*) or pERK (*Bottom*). No clear difference in pAKT or pERK immunostaining was noted, consistent with the results from Western blotting shown in Fig. S1.

Forestomach
Glandular stomach
Fold Change
1.5
1.0
0.5
0.0
Keratin 5
Progastricsin
Marker

Forestomach
Glandular stomach
Ras mRNA levels (vs Glandular Stomach)
9
8
7
6
5
4
3
2
1
0
Hras
Kras
Nras
Ras Isoform

Fig. S3. Expression of Ras isoforms in epithelial cells of the forestomach and glandular stomach. The appropriate cell layer was isolated from frozen sections of stomachs of control mice by laser capture microdissection. (*Left*) Expression of progastricsin and keratin 5 as determined by RT-PCR. Data are plotted relative to the expression of keratin 5 or progastricsin in forestomach and glandular stomach, respectively, and confirm appropriate enrichment of the corresponding cell types. (*Right*) Relative expression of Ras isoforms in squamous and glandular gastric epithelial cells. Data are plotted relative to expression of the respective Ras isoform in glandular stomach. GAPDH was used as a standard.

Fig. S4. Loss of WT *Hras* allele in papillomas arising in *CC/FR-Hras*^{G12V} mice. We performed semiquantitative PCR using primers that amplify only the WT *Hras* allele in papillomas of *CC/FR-Hras* ^{G12V} mice. Nontumor tissues of *CC/FR-Hras* ^{G12V} mice were used as a reference, and GAPDH as a loading control. The WT *Hras* allele in an index nontumor tissue was normalized to one after quantification on a 1% agarose gel. The WT *Hras* copy number in 3 of the 7 papillomas was markedly lower compared to control, indicative of loss of this allele. The WT *Hras* allele in the papilloma with *Hras* amplification illustrated in Fig. 4*C* was not deleted. These data were confirmed by selective amplification of the WT *Hras* allele after EcoRV digestion of the mutant *Hras* gene (not shown)

Fig. S5. Papillomas arising in *CC/FR-Hras*^{G12V} mice express markers of DDR and senescence. (*A*) IHC staining of skin (*Top*) and of a papilloma sections (20×) (*Bottom*) with antibodies to p53 and γH2AX. Nuclear staining is apparent in squamous cells from papilloma, but not from the adjacent epidermis. Staining with SA-βgal revealed positive cells in hair follicles and sebaceous glands, which is known to occur in an age-independent fashion in normal dermis. However, there was no SA-βgal staining in papillomas. Squamous cells from papillomas did show robust positivity for p19. (*B*) Expression of senescence markers in papillomas of *CC/FR-Hras* ^{G12V} mice. Because IHC for other senescence markers (i.e., p16) was not informative, we performed Western blots of mouse skin tissue from *CC/FR-Hras*^{G12V} and of individual papillomas for the indicated proteins. Expression of p53, p19, p21, and p16 was increased in tumors compared to uninvolved skin.

Fig. S6. Effects of endogenous expression of Hras^{G12V} on growth and signaling of MEFs. (*A*) Cumulative cell number from serial passage of 3 independent MEF preparations from *CC/FR-Hras^{G12V}* and control mice. (*B*) Short-term growth curves of MEFs with or without endogenous expression of Hras^{G12V} at passage 3 or 15 (*C*). Data represent mean ± SEM of 3 independent MEF preparations for each cell type and passage. (*D*) Western blots of lysates of early- and late-passage *Hras^{m}*-MEFs and *Hras^{wt}*-MEFs treated with 10 ng/ml FGF for the indicated time, probed with antibodies against pAKT, pERK1/2, or tAKT or β-actin. Late-passage MEFs show an attenuated response to FGF, which is less apparent in *Hras^{m}*-MEFs, consistent with escape from senescence. Similar findings were seen in 2 additional paired *Hras^{m}* and *Hras^{wt}* lines. (*E*) Western blots of lysates of late-passage *Hras^{m}*-MEFs and *Hras^{wt}* MEFs treated with 0.5 μM of doxorubicin for 6 h, probed with antibodies against p53, phospho-ser15 p53, p21, p19, γ-H2AX, or β-actin. (*F*) Over-expression, but not endogenous expression of Hras^{G12V} cooperates with Myc or T antigen to transform MEFs. Early passage *Hras^{m}*-MEFs and *Hras^{wt}*-MEFs were transduced with retroviral vectors expressing Myc, large T antigen (Tag) with or without Hras^{G12V} for 48 h. Transduced cells (0.5×10^6) were plated on 10-cm plates, and scored for colony development after 14 days. Bars show that cells over-expressing Hras cooperate with Myc or Tag to induce colony formation, whereas MEFs expressing endogenous Hras are not transformed by either oncogene.